Event-based camera refractory period characterization and initial clock drift evaluation

McMahon-Crabtree, Peter N ; Kulesza, Lucas ; McReynolds, Brian ; O'Keefe, Daniel S ; Puttur, Anirvin ; Maestas, Diana ; Morath, Christian P ; McHarg, Matthew G

Abstract: Event-based camera (EBC) technology provides high-dynamic range operation and shows promise for efficient capture of spatio-temporal information, producing a sparse data stream and enabling consideration of nontraditional data processing solutions (e.g., new algorithms, neuromorphic processors, etc.). Given the fundamental difference in camera architecture, the EBC response and noise behavior differ considerably compared to standard CCD/CMOS framing sensors. These differences necessitate the development of new characterization techniques and sensor models to evaluate hardware performance and elucidate the trade-space between the two camera architectures. Laboratory characterization techniques reported previously include noise level as a function of static scene light level (background activity) and contrast responses referred to as S-curves. Here we present further progress on development of basic characterization methods and test capabilities for commercial-off-the-shelf (COTS) visible EBCs, with a focus on measurement of pixel deadtime (refractory period) including results for the 4th-generation sensor from Prophesee and Sony. Refractory period is empirically determined from analysis of the interspike intervals (ISIs), and results visualized using log-histograms of the minimum per-pixel ISI values for a subset of pixels activated by a controlled dynamic scene. Our tests of the Prophesee gen4 EVKv2 yield refractory period estimates ranging from 6.1 msec to 6.8 μsec going from the slowest (20) to fastest (100) settings of the relevant bias parameter, bias_refr. We also introduce and demonstrate the concept of pixel bandwidth measurement from data captured while viewing a static scene – based on recording data at a range of refractory period setting and then analyzing noise-event statistics. Finally, we present initial results for estimating and correcting EBC clock drift using a GPS PPS signal to generate special timing events in the event-list data streams generated by the DAVIS346 and DVXplorer EBCs from iniVation.

DOI: https://doi.org/10.1117/12.2672301

Event-Based Camera Refractory Period Characterization and Initial Clock Drift Evaluation

Peter N. McMahon-Crabtree*[a], Lucas Kulesza[a], Brian J. McReynolds[c], Daniel S. O'Keefe[b], Anirvin Puttur[b], Diana Maestas[a], Christian P. Morath[a], and Matthew G. McHarg[a]
[a]Air Force Research Laboratory, 3550 Aberdeen Ave. SE, Albuquerque, NM, USA 87117;
[b]U.S. Air Force Academy, Space Physics and Atmospheric Research Center, Department of Physics and Meteorology, 2354 Fairchild Dr., USAFA, CO, USA 80840;
[c]Institute of Neuroinformatics, UZH/ETH Zurich, Sensors Group, 190 Winterthurerstrasses, 8057 Zurich, Switzerland

ABSTRACT

Event-based camera (EBC) technology provides high-dynamic range operation and shows promise for efficient capture of spatio-temporal information, producing a sparse data stream and enabling consideration of nontraditional data processing solutions (e.g., new algorithms, neuromorphic processors, etc.). Given the fundamental difference in camera architecture, the EBC response and noise behavior differ considerably compared to standard CCD/CMOS framing sensors. These differences necessitate the development of new characterization techniques and sensor models to evaluate hardware performance and elucidate the trade-space between the two camera architectures. Laboratory characterization techniques reported previously include noise level as a function of static scene light level (background activity) and contrast responses referred to as S-curves. Here we present further progress on development of basic characterization methods and test capabilities for commercial-off-the-shelf (COTS) visible EBCs, with a focus on measurement of pixel deadtime (refractory period) including results for the 4th-generation sensor from Prophesee and Sony. Refractory period is empirically determined from analysis of the interspike intervals (ISIs), and results visualized using log-histograms of the minimum per-pixel ISI values for a subset of pixels activated by a controlled dynamic scene. Our tests of the Prophesee gen4 EVKv2 yield refractory period estimates ranging from 6.1 msec to 6.8 μsec going from the slowest (20) to fastest (100) settings of the relevant bias parameter, *bias_refr*. We also introduce and demonstrate the concept of pixel bandwidth measurement from data captured while viewing a static scene – based on recording data at a range of refractory period setting and then analyzing noise-event statistics. Finally, we present initial results for estimating and correcting EBC clock drift using a GPS PPS signal to generate special timing events in the event-list data streams generated by the DAVIS346 and DVXplorer EBCs from iniVation.

Keywords: Event-based cameras, sensor characterization, dynamic vision sensors, neuromorphic imaging, asynchronous imaging

1. INTRODUCTION

Neuromorphic vision (or event-based) sensor device research began in Carver Mead's laboratory at the California Institute of Technology around 1986, with the 1992 thesis of Misha Mahowald winning the university's Clauser Prize [1-2]. Commercial-off-the-shelf (COTS) event-based cameras (EBCs) are now available from multiple vendors [2], including iniVation (Switzerland) and Prophesee (France), to include the HD format (720x1280 pixels) 4th-generation model from Prophesee in collaboration with Sony [2-3]. Event-based sensing is of interest for low-SWaP machine vision and autonomous systems and is also being explored for long-standing remote sensing challenges such as space domain awareness (SDA) [2, 4-5]. Unlike well-developed and standardized methodologies to characterize CCD/CMOS framing cameras [6-8], complementary methodologies appropriate for EBCs are still in research and development [9-11]. Additionally, few assessments of radiation tolerance of COTS EBC technology are reported in the literature [12-13]. Test and evaluation of environmental survivability and systematic comparison of EBC hardware requires a repeatable test setup and methodology. Here we report work on analyzing the event-list data focused on interspike interval (ISI) statistics [14-15] to estimate pixel deadtime (refractory period) and potentially garner an indirect measure of front-end pixel bandwidth.

Characterization of standard CCD/CMOS framing sensors involves recording both dark frames and flat fields while varying sensor integration time. A series of dark frames collected at a set of integration times provides a measure of dark current (ADUs/second). A series of flat fields collected at several radiometric light levels and/or a single radiometric light

Approved for public release; distribution is unlimited. Public Affairs release approval #AFRL-2023-2933
*Corresponding author: AFRL.RVSU.BranchTasker@us.af.mil

level while varying integration time enables calculation of the photon transfer curve providing a measure of well-depth (ADUs), read noise (ADUs), and conversion gain (e-/ADU). Event-sensors do not integrate signal in an explicitly controllable fashion – but similar characterization is required in terms of collecting data at fixed light levels, while varying event-sensor bias settings (pixel bandwidths, refractory period, contrast thresholds). Additionally, as EBC pixels are fundamentally asynchronous change detectors, a dynamic light source is typically utilized to measure bandwidth and contrast threshold [9-10, 16] – a key difference compared to CCD/CMOS framing cameras. In this paper we explore the utility of sweeping refractory period while viewing both static and dynamic scenes. For the case of a static scene, we consider monitoring noise-event statistics [15] with the goal being to extract an estimate of front-end pixel bandwidth. For the case of a dynamic scene, we consider the mean minimum ISI within a subset of pixels activated by a relatively slow stimulus, with the goal being to measure the physical pixel deadtime as a function of the abstracted refractory period bias setting.

The overarching goal of this project is to develop initial test capabilities and sensor models to evaluate and characterize COTS visible EBCs enabling systematic comparisons between various EBC makes and models, as well as between EBCs and traditional framing cameras. Section 2 provides EBC background including a basic description of noise behavior and performance characterization. Our EBC test stations and methodologies are described in Sect. 3. Section 4 presents refractory period estimation results for the Prophesee gen4 EVKv2 and gen4 EVKv3 models. Additionally, Sect. 4 presents initial simulation and measurement results validating the concept of using noise-event statistics (de-coupling) to gain insight into pixel bandwidth. Section 4 concludes with our initial results for EBC clock drift measurement and correction for the iniVation DAVIS346 and DVXplorer models. Finally, a summary and discussion of results is presented in Sect. 5.

2. BACKGROUND

2.1 Description of Event-Based Cameras

Event-based sensors (also known as neuromorphic vision sensors or silicon retinas or dynamic vision sensors) are biology-inspired devices comprised of an array of pixels that continuously monitor log-photocurrent and asynchronously respond to changes therein, defined as temporal contrast (TC) [2, 17]. The three main components of the EBC pixel unit cell are a log-photoreceptor, differencing circuit, and comparator, which are tunable via six primary biases influencing the photoreceptor, source follower (buffer), change amplifier, contrast thresholds, and refractory period (pixel deadtime) [18]. A given EBC pixel generates a positive event when the following condition is satisfied:

$$\ln\left(\frac{I_{pho}(t_1)}{I_{pho}(t_0)}\right) \geq \theta_{ON} \tag{1}$$

whereas a negative event is generated when the following is satisfied:

$$\ln\left(\frac{I_{pho}(t_1)}{I_{pho}(t_0)}\right) \leq \theta_{OFF} \tag{2}$$

where I_{pho} is photocurrent, t_1 is current time, t_0 is time of last pixel reset, and θ_{ON} and θ_{OFF} are positive- and negative-going thresholds, respectively. When a new event is generated at time t_1, the current time is recorded, and the output of an EBC is a stream of N events e_i:

$$e_i = \{(x,y)_i, p_i, t_i\}_{i=1\ldots N} \tag{3}$$

where each event is described by pixel position $(x,y)_i$, timestamp t_i (to the nearest microsecond for currently available hardware), and polarity $p_i \in \{-1,+1\}$. The polarity indicates whether photocurrent was increasing or decreasing.

2.2 Event-Based Camera Noise Behavior and Performance Characterization

Event-based cameras are quite different from typical framing sensors. They are basically asynchronous imaging change detectors, and thus a different approach to characterization is required.

Framing sensor/camera behavior is characterized using the photon transfer curve technique based on collecting dark frames and flat fields at a range of light levels and/or integration times. The goal being to characterize and quantify the sensor's ability to accurately report the number of photoelectrons collected over a given integration time. Integration time, frame rate, and conversion gain are parameters typically controlled by the end-user of a framing camera. Event-based camera pixels independently respond to changes in log-photocurrent. The change detection thresholds (positive and negative), pixel bandwidth, and refractory period can be tuned over some range via on-chip bias current generators. Behavior of state-of-the-art event-based sensors as reported in the literature is characterized by the background activity (BA), contrast

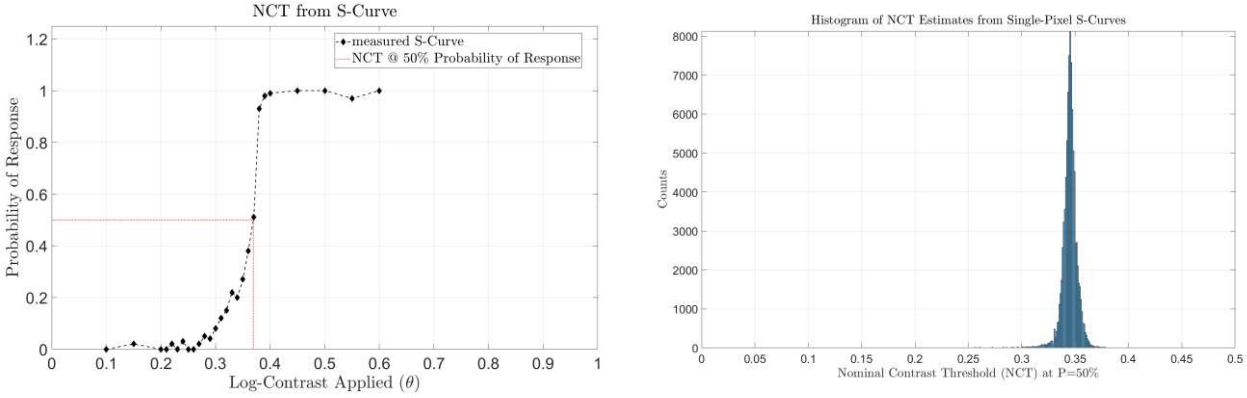

(a) Example single-pixel NCT from S-curve (b) Example histogram of single-pixel NCT estimates

Figure 1. (a) Example single-pixel S-curve and resulting NCT estimate measured for DAVIS346 SN 0498 by programmatically driving the SpectralLED light source to generate a slow train of 100 positive pulses (1.67 Hz). (b) Example histogram of single-pixel NCT estimates measured across the full EBC FPA, indicating a mean NCT near 35%.

response probability S-curves from which a nominal contrast threshold (NCT) is derived, low-light cut-off (LLCO) and dynamic range (DR), and contrast threshold non-uniformity (CTNU) [3].

For a given baseline light level (steady state photocurrent) and given camera noise characteristics and bias settings, there is some probability that a positive-polarity or negative-polarity noise event will be generated. This false alarm probability is described by the BA curve which gives noise events rates (events per second per pixel) as a function of static scene light level. The BA curve is driven by shot noise events (SNEs) at the low-end of DR while leakage events dominate at high light levels for 3rd-generation and earlier dynamic vision sensor (DVS) designs [11, 19-20]; although the latest generation event-sensor design from Prophesee and Sony mitigates leakage activity [3]. As an example, we previously measured and reported the dark noise and BA curve pre-irradiation for DAVIS346 serial number (SN) 0497 [13], where the BA was bounded between about 3.0 and 0.07 events/sec/pixel (eps/pixel) for on-chip light levels ranging from approximately 50 mlux to 1 klux (at default bias settings determined by the DV software). By comparison, Prophesee and Sony report a BA for their latest sensor which is bounded between about 8.3 and 0.005 eps/pixel for on-chip light levels ranging from 1 mlux to 100 klux.

In terms of temporal contrast sensitivity, EBC performance is described by its response to an applied stimulus. The EBC response (mean number of events generated per pulse or probability of at least a single event generated per pulse) is plotted versus stimulus amplitude – yielding an S-curve [10, 21]. The S-curve is measured on a pixel-by-pixel basis at a given baseline light level, with the 50% probability point typically reported as the NCT [3] for a specified on-chip light level. An example single pixel S-curve we previously measured for the DAVIS346 SN 0498 is shown in Figure 1(a), including a red dotted line indicating the NCT. A slow pulse train was applied to the entire DAVIS346 FPA yielding an NCT measurement for each pixel – an example histogram of single pixel NCTs is presented in Figure 1(b) describing the CTNU [13]. The EBC pixel temporal bandwidth is typically measured in a similar fashion in terms of response (mean events/cycle) to a periodic signal of increasing frequency [9-10, 16].

Literature describing the 4th-generation event-sensor from Prophesee and Sony does not address refractory period [3]. The Prophesee MetaVision SDK documentation describes bias settings including the parameter *refr_bias* (refractory period), but does not relate the allowable range of *bias_refr* values to a range of physical deadtimes [22]. Prior work of one of us (B. McReynolds) describes a procedure to measure: (1) temporal contrast threshold, (2) temporal cutoff frequency, and (3) refractory period [10]. The procedure of [10] for measuring refractory period applies a slow square wave stimulus, finds the time in each pixel between the first two (+) events generated at each rising edge (Δt_{meas} or ISI_{meas}), then uses a simplified DVS pixel circuit model along with separate measurements of cutoff frequency (f_{3dB}) and contrast threshold (θ_{ON}) to infer refractory period as $t_{refr} = \Delta t_{meas} - \Delta t_{ideal}$.

2.3 On the value of accurate timing information for space awareness applications

Understanding the timing characteristics and performance of event-based sensors as well as packaged cameras, such as available COTS hardware from iniVation and Prophesee, is of paramount importance for applications such as astronomy

(a) Prophesee gen4 EVKv3 (b) iniVation DAVIS346 (c) iniVation DVXplorer

Figure 2. Commercially available event-based cameras used for studies reported in this paper.

and SDA/space traffic management. In terms of natural scene sparsity, event-based sensing is well-suited for application to a subset of SDA tasks where higher temporal resolution measurements (compared to what is currently provided by CMOS framing sensors) may provide additional information about the orbits and characteristics of manmade space objects [4-5]. However, key limitations of currently available COTS EBCs from the SDA perspective include high noise rates when viewing a dark scene, and challenges to measuring absolute time for each detected change event. While EBC manufacturers advertise microsecond temporal precision as a key advantage of neuromorphic sensors, utility of the relatively high time resolution information is degraded if the event data stream cannot be accurately calibrated to absolute time. Our initial measurements of clock drift for several COTS EBCs from iniVation, including results for simple mean drift correction, are presented in Sect. 4.

3. METHODOLOGY

3.1 Event-Camera Hardware

Several EBCs were acquired for test and evaluation, including the gen4 EVKv2 and gen4 EVKv3 models from Prophesee, and the DAVIS346 and DVXplorer models from iniVation (see Figure 2). Basic specifications for the devices are provided in Table 1 [2].

Table 1. Specifications for a subset of commercially available event-based cameras.

Manufacturer:	**iniVation**		**Prophesee**	
Camera Model:	**DAVIS346**	**DVXplorer**	**gen3 VGA-CD**	**gen4 HD-CD**
Format (pixels)	346x260	640x480	640x480	1280x720
Minimum Contrast Sensitivity (%) such that 50% of pixels respond	14.3 (on) and 22.5 (off)	13	12	11
Power Consumption – Sensor (mW)	10-170	27-50	36-95	32-84
Pixel Pitch (μm)	18.5	9	15	4.86
Fill Factor (%)	22	unknown	25	>77
Supply Voltage (V)	1.8 and 3.3	1.2, 1.8 and 2.8	1.8	1.1 and 2.5
CMOS Technology	180 nm 1P6M	90 nm BSI CIS	180 nm 1P6M	90 nm BSI CIS
Max Readout Bandwidth (Meps)	12	165	66	1066
Interface	USB 3	USB 3	USB 3	USB 3

3.2 Using a controlled dynamic scene to observe impact of the refractory period bias setting

In concept, the pixel refractory period is a simple characteristic. However, for currently available COTS VIS EBCs, the relationship between the abstracted refractory period bias setting and physical deadtime is not provided except for the opensource jAER software which provides nominal design values for the DAVIS346. These were shown in [10] to vary significantly from real world performance, and the correction to the jAER software based on an improved circuit model and empirical results is pending. Because refractory period measurements are not included in manufacturer specifications,

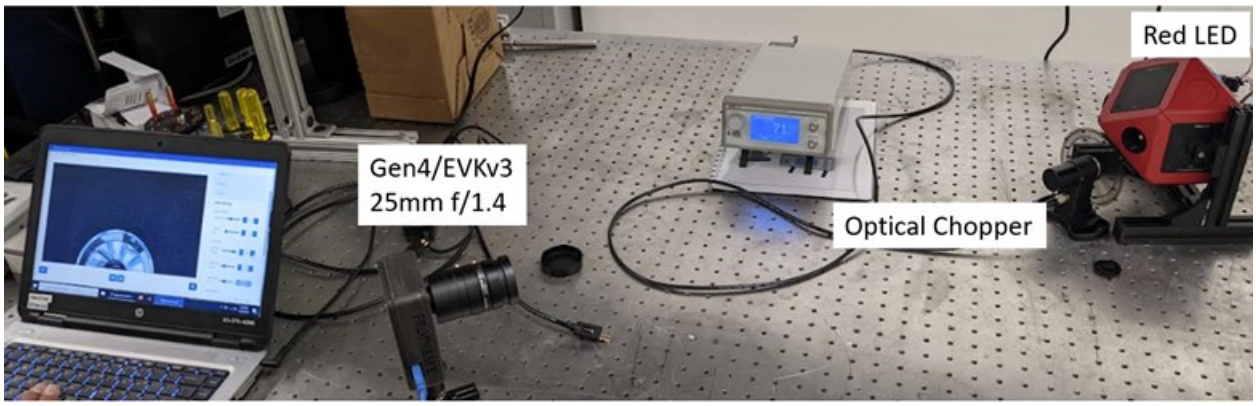

Figure 3. Experiment setup at USAFA including chopper wheel placed between event-based camera and integrating sphere (frequency generator/power source for LED not shown). The large blades of the chopper wheel are applying either a 20 Hz or 4 Hz modulation to the static light source. The integrating sphere light source was either a red or bright white LED.

a complete EBC test sequence should include measurements of physical refractory period as a function of bias setting. The approach to measuring refractory period taken in this paper does not rely on either (1) a simplified DVS pixel circuit model, or (2) separate measurements of pixel bandwidth and contrast threshold, as does one previously reported approach [10]. To make this simplification, we assess that (1) the temporal response of the photoreceptor circuit is very fast relative to the refractory period, and (2) the thresholds are quite small. The first assumption is valid provided that background light level is high (greater than about 100 lux) and both photoreceptor and source follower biases are set at least to a moderately high level compared to the baseline default value. The second condition is achieved by tuning the threshold levels.

Impact of the refractory period bias setting can be observed by viewing a controlled dynamic scene using a slow stimulus such as a square wave signal driving an LED or placing a chopper wheel in front of a static light source. We initially used the USAFA laboratory setup shown in Figure 3 comprised of either a red LED or bright white LED as static input to an integrating sphere, and a chopper wheel imposing either a 20 Hz or 4 Hz modulation on the light source. The Prophesee gen4 EVKv3 with 25 mm f/1.4 lens is focused on the output port of the integrating sphere seen through the chopper wheel, where the separation between camera and integrating sphere is roughly 80 cm.

The six bias settings that are adjustable using the manufacturer provided MetaVision software are described in Table 2 below [22]. The contrast thresholds are adjusted (defined) based on the differences (*bias_diff_on – bias_diff*) and (*bias_diff – bias_diff_off*), where the manufacturer recommends the value of *bias_diff* remain fixed at default. The contrast thresholds can only be within 15 of *bias_diff*, defining maximum sensitivity (minimum thresholds). The foundational DVS pixel circuit front-end bandwidth increases monotonically with the photoreceptor and buffer bias currents, and with photocurrent [18]. For the Prophesee gen4 EVKv2 and EVKv3, the pixel bandwidth is controlled by *bias_fo* (low-pass filter) and *bias_hpf* (high-pass filter). An additional parameter *bias_pr* (not listed in Table 2) controlling the photoreceptor bias is adjustable for the gen3 but is not accessible for the gen4/gen4.1/IMX636/IMX637 models.

To observe the impact of changing refractory period, the *bias_fo* and *bias_hpf* parameters were initially set to maximize bandwidth of unit cell circuitry "up-stream" from the change detection reset circuit. The change detection thresholds *bias_diff_on* and *bias_diff_off* were also set to maximize sensitivity. Data was then collected at 8 or 9 different values of *bias_refr*: [30, 40, …, 100] or [20, 30, …, 100]. The assumption is now that given sufficient light-level and with arbiter/readout bandwidth not a limiting factor, the mean minimum ISI will provide a measure of the refractory period.

Table 2. Summary of Prophesee gen4.1 bias parameters including configuration for evaluating the refractory period setting.

Bias Parameter	**Default Value**	**Minimum Value**	**Maximum Value**	**Test Configuration Values**	**Comment**
bias_fo	74	45	110	110	low-pass filter
bias_hpf	0	0	120	0	high-pass filter
bias_diff	80	52	100	80	(recommended to not adjust)
bias_diff_on	115	bias_diff + 15	140	95	threshold for ON events
bias_diff_off	52	25	bias_diff - 15	65	threshold for OFF events
bias_refr	68	20	100	[20, 30, …, 100]	refractory period

bias_refr = 30 (slow/long refractory period)

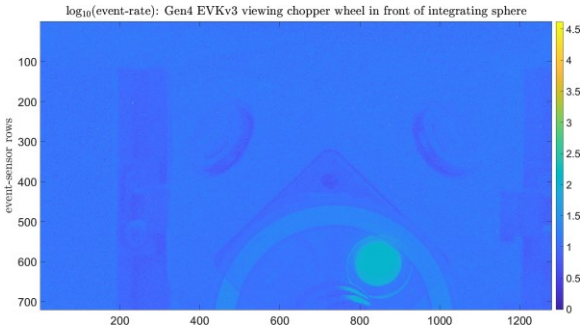

(a) mean event-rate across full data set = 17.4 eps/pix

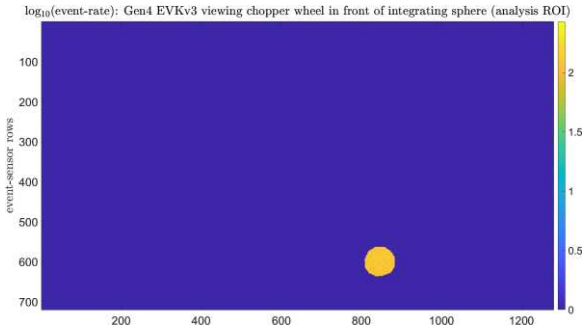

(b) mean event-rate across analysis ROI = 124.3 eps/pix

bias_refr = 100 (fastest/smallest refractory period)

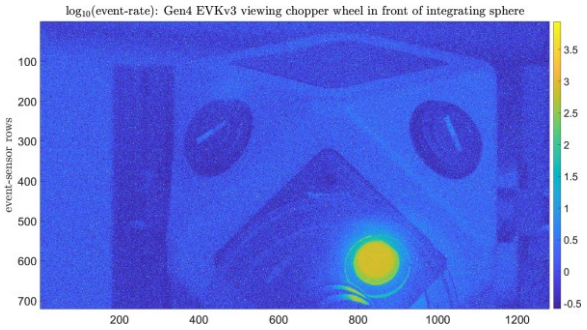

(c) mean event-rate across full data set = 21.7 eps/pix

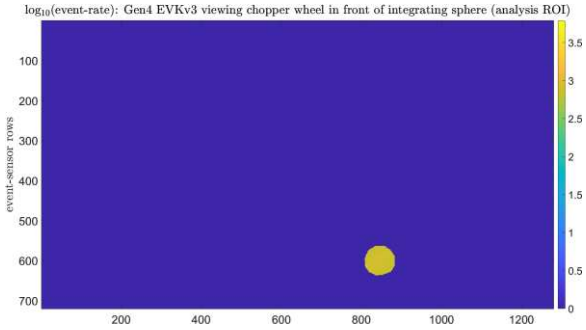

(d) mean event-rate across analysis ROI = 803.4 eps

Figure 4. Visualizations of data captured by gen4 EVKv3 viewing 20 Hz chopper wheel in front of integrating sphere illuminated by a red LED source are shown in (a) and (c). The analysis ROI created for post-processing is shown in (b) and (d), along with the average event rate within the ROI for these two refractory period settings.

Furthermore, we propose that if one empirically determines the point where increasing light level no longer results in lowering of the mean minimum ISI (vs. *bias_refr*) curve, this crossover point may provide additional insight into the event-based sensor behavior. Measuring this crossover point (in terms of an on-chip irradiance/illuminance and estimate of photocurrent given availability of a QE curve) is a potential component of a future standardized EBC characterization protocol – describing the transition from front-end bandwidth to refractory period as limiting the minimum per-pixel (sampling) time between events.

Additionally, the latest gen4/gen4.1/IMX636/IMX637 models provide some or all the following on-chip event signal processing functions [22], which are also adjustable using the MetaVision software: Anti-Flicker (AFK), Event Trail Filter (STC/Trail), and Event Rate Controller (ERC). The ERC enables dynamic event dropping to limit max throughput to the target event rate. Finally, the MetaVision software provides a Region of Interest (ROI) selection feature allowing one to record data from only a subregion of the full FPA.

For initial testing of our approach, 8 data files were recorded for *bias_refr* values of [30, 40, … , 100], with other biases set to those values listed in Table 2, using the red LED and chopper wheel set to 20 Hz. The ROI selection feature was disabled so that event data from all pixels was recorded, and the on-chip processing functions were left at default. The average event rate image (2D histogram summing events over time) was generated from each data file to provide basic data visualization, and the two resulting images for the slowest (30) and fastest (100) refractory periods exercised are shown in Figure 4a and Figure 4c, respectively. Next, an analysis ROI was manually created in MATLAB to constrain the ISI analysis to only those pixels imaging the integrating sphere output port while being modulated by the chopper wheel (see Figure 4b and Figure 4d). Figure 4 also provides mean event rates for the min and max refractory period settings exercised, for the entire image and for just the analysis ROI. The relative change (increase) in mean event rate within the ROI in this case is a factor of about 5.5 going from *bias_refr*=30 to *bias_refr*=100, whereas the relative increase in mean event rate for the entire FPA is about 0.25.

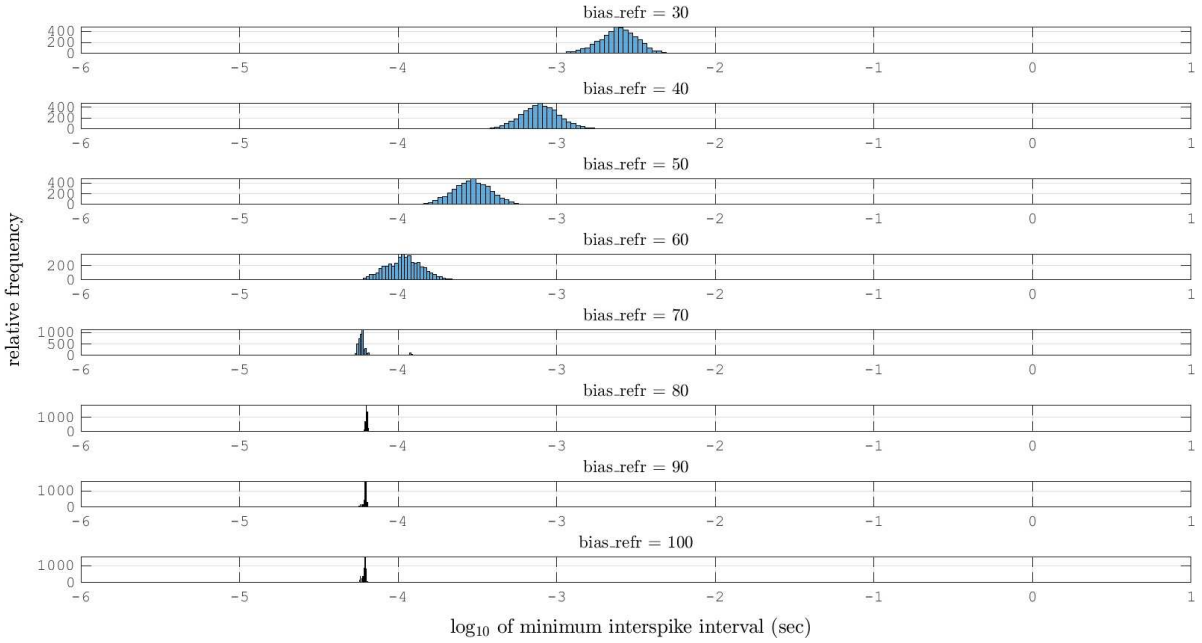

Figure 5. Base-10 log-histograms of minimum per-pixel ISIs within the analysis ROI, for values of *bias_refr* ranging from slow (30) at top to the fastest setting (100) at bottom. The analysis ROI covers 4441 pixels or 0.5% of the full FPA.

The ISIs were calculated on a per pixel basis and a log-histogram of the resulting per-pixel minimum ISIs within the analysis ROI is displayed in Figure 5 for each *bias_refr* value examined. The mean value of the minimum per-pixel ISIs within the analysis ROI is plotted versus refractory period bias setting in Figure 6 (blue diamonds). The total mean event

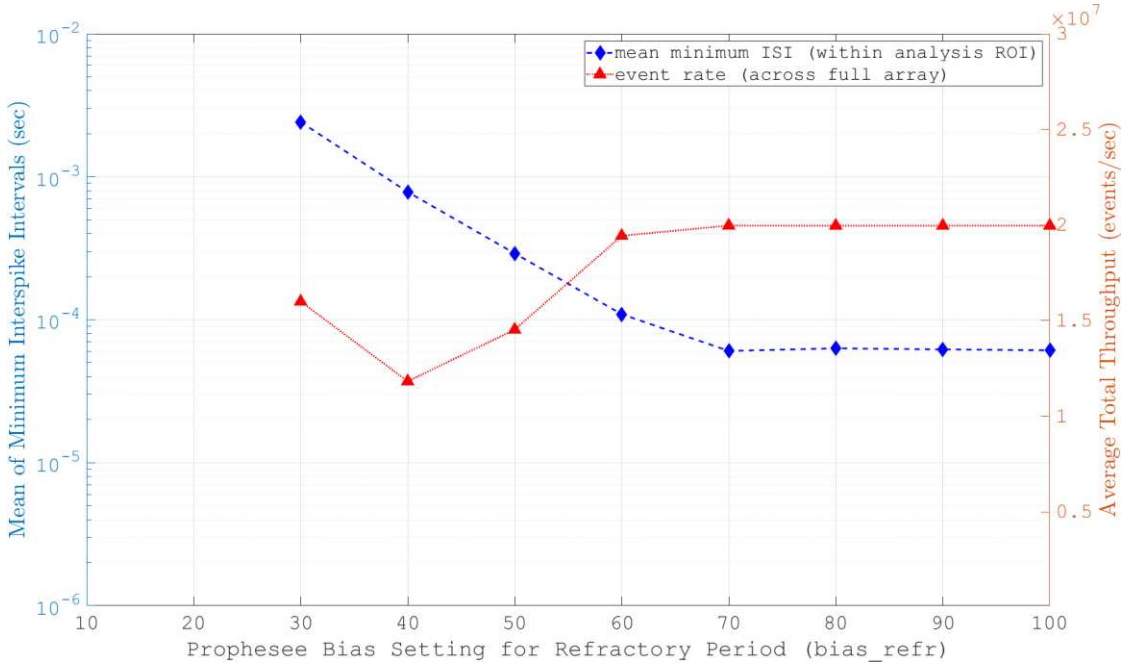

Figure 6. The mean minimum interspike interval within the analysis ROI is plotted (blue diamonds) versus refractory period bias setting, *bias_refr*. Total average event rate is also plotted (red triangle) versus *bias_refr*. The analysis ROI covers 4441 pixels or 0.5% of the total array.

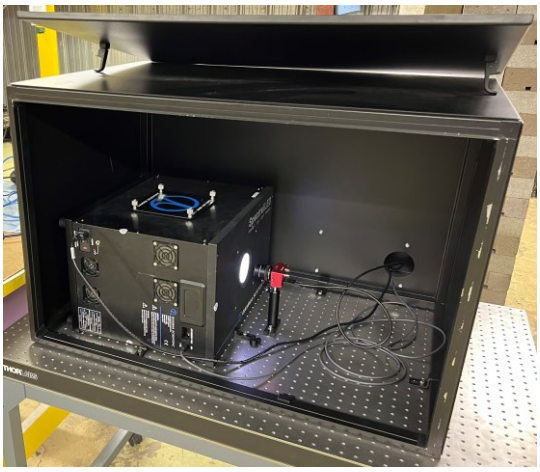

(a) Mobile test station for evaluating COTS VIS EBCs

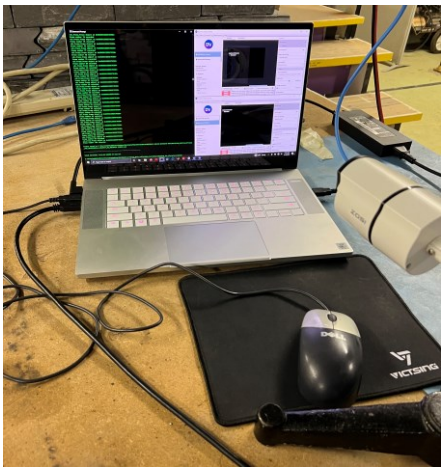

(b) Laptop with custom Python code for automation

Figure 7. Mobile test station for automated characterization of COTS visible EBCs: (a) DAVIS346 with 25 mm f/4.0 lens viewing the SpectralLED light source, and (b) Laptop used for test station hardware control and data acquisition.

rate is also plotted versus *bias_refr* (red triangles) to gain insight into state of the event readout/arbiter. Note that mean minimum ISI (within analysis ROI) decreases with roughly linear steps on a semi-log (y-axis) plot from *bias_refr* = 30 to *bias_refr*=60, then saturates near 60 µsec for *bias_refr* ≥ 70. Based on visual inspection, the saturation point for mean min ISI coincides with saturation of mean event throughput at a value near 20 Meps. The advertised maximum sustained readout bandwidth of the Prophesee/Sony gen4 is 1.066 Geps [3]. However, the default setting for the on-chip ERC is 20 Meps – consistent with Figure 6. The result of Figure 6 does not necessarily describe physical refractory period, but, again, we assume that given the correct bias settings and test conditions (sufficient light level and modulation while avoiding readout saturation) the results of this approach will yield meaningful estimates of the reset circuit deadtime.

Complementary refractory period evaluation of the gen4 EVKv2 was performed in a separate laboratory (at AFRL) using our mobile test station (see Figure 7) assembled to evaluate COTS EBCs from iniVation and Prophesee. Our test station is composed of a radiometrically calibrated and tunable Lambertian source (SpectralLED RS-7-1 from Gamma Scientific), a light-tight enclosure (from VERE), a single Edmund Optics 25 mm f/4.0 double Gauss lens (part #55326), and a laptop for hardware control and data acquisition. The 25 mm f/4.0 lens was used for all measurements other than for dark noise or dark current, in which case the lens was removed, and the camera body cap reattached. We wrote custom Python code to control the SpectralLED integrating sphere (Serial over USB), and COTS EBCs from iniVation and Prophesee – dependent on the DV software from iniVation and the MetaVision software from Prophesee. In addition to programmatic adjustment of light level, the Python code can also request the current SpectralLED light level (luminance and spectral radiance) be saved to a *.CSV file.

3.3 Approach to measuring front-end pixel bandwidth using a static scene

Event-based camera pixel bandwidth is typically measured by viewing a dynamic scene composed of an LED modulated with a periodic signal such as a sine wave or triangle wave, then monitoring the average number of events generated per cycle as a function of modulation frequency [10, 16]. This requires a well calibrated light source capable of achieving very fast modulation frequencies. A much simpler alternative approach to measuring pixel bandwidth is based on viewing a static scene and monitoring noise event statistics as a function of refractory period bias setting. The basic idea is that front-end pixel bandwidth will impose a correlation (coherence) time on the in-pixel noise current/voltage, with correlation time being inversely proportional to bandwidth. In the case where refractory period is less than the correlation time, we expect an abundance of noise-event pairs with opposite polarity as shown in [15]. When a positive-polarity (or negative-polarity) event is generated under this condition, the probability of the following event being opposite polarity is high because the reset level will be above (or below) the present (short timescale) mean current/voltage which remains approximately constant during the correlation time. When the refractory period becomes larger than the correlation time the event-pairs become de-coupled, and we expect the fraction of opposite polarity events to drop from near one to 50%. We also expect

Table 3. Summary of noise event de-coupling times for several DVS pixel bandwidth values. The de-coupling time was estimated using Monte Carlo simulations of a DVS pixel.

Cutoff Frequency, f_{3dB} (Hz)	Time Constant, τ_{3dB}	De-Coupling Time, $4*\tau_{3dB}$
10	15.9 msec	63.7 msec
100	1.6 msec	6.4 msec
637	250 µsec	1 msec
1k	159 µsec	637 µsec
10k	15.9 µsec	63.7 µsec

both the correlation coefficient between ON and OFF noise event rates, and the overall event rate, to drop in a non-linear fashion as the noise event pairs become de-coupled. As proposed by McReynolds, *et al.*, this break point represents an approach to managing EBC SNEs [10], but also motivates this potential alternate approach to measuring pixel bandwidth.

Based on Monte Carlo simulations of a single DVS pixel using a custom tool like the open-source DVS simulator V2E [20], we found that the refractory period must be about $4 \times \tau_{3dB}$ (where $\tau_{3dB}=1/(2\pi f_{3dB})$) to observe the de-coupling such that the fraction opposite polarity falls to 50%. Therefore, we need pixel bandwidth of roughly several hundred Hz or greater to observe de-coupling (see Table 3) with the gen4 EVKv2 given the achievable range of refractory periods (see results in Section 4).

3.4 Measurement of EBC Clock Drift

The test setup to measure COTS EBC clock drift was comprised of a Time Machines (TM) 1000A GPS receiver, a custom-built cable (HR10A Push-Pull connector) to interface with the EBC trigger (sync) input, and a DC 5V power supply (see Figure 8). The DC power supply was wired to the trigger input interface to provide a continuous supply voltage to the camera, enabling signal detection, while the other pins were connected to the serial output of the GPS receiver and ground (see Figure 8). An oscilloscope was used to verify the input of pulse-per-second (PPS) TTL pulses from the GPS receiver. The DV software from iniVation was used to activate generation of special timing events given an appropriate signal

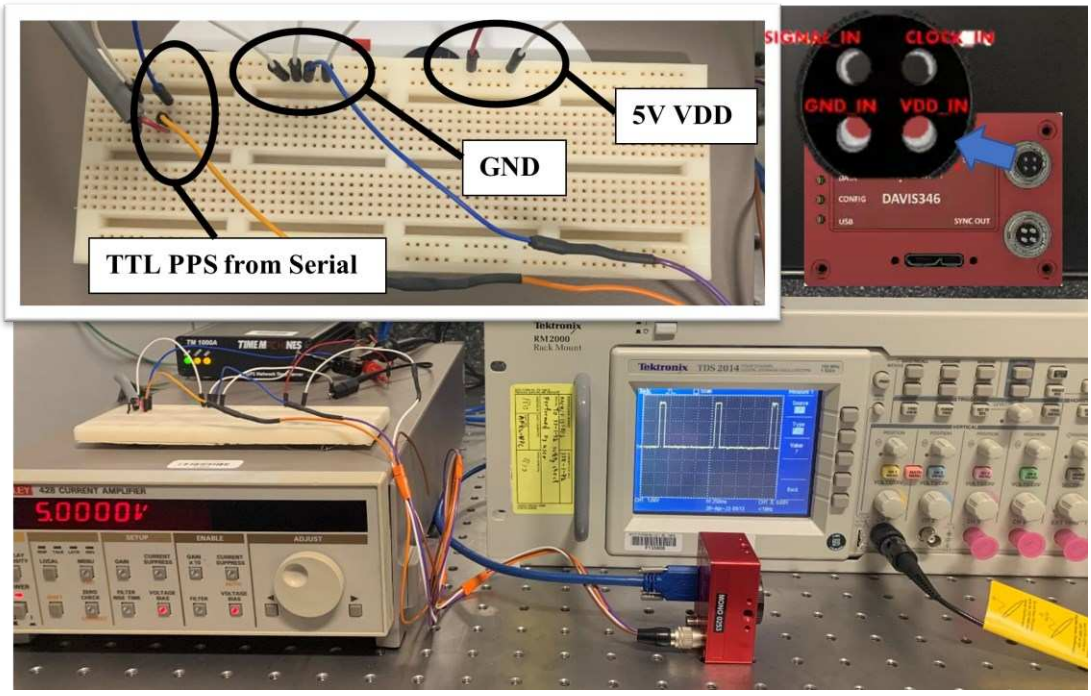

Figure 8. Test setup used to measure clock drift of several iniVation EBCs. The 5V DC supply is wired to the EBC VDD_IN, GND to GND_IN, and PPS signal (via serial cable) to SIGNAL_IN. Top left: detailed view of wiring. Top right: diagram of DAVIS346 trigger input pin connections from https://inivation.com/wp-content/uploads/2019/08/DAVIS346.pdf.

directed to the EBC trigger input port, and then subsequently used to record timing events generated by the EBC electronics at the rising edge of each detected TTL pulse. Each trigger event consists of two components: a timestamp in Unix epoch time synced to the computer clock at the beginning of each recording, and a "type" designation that denotes detection of a rising edge (1) or falling edge (0). Trigger data sets were typically recorded over a period of 24 hours for each COTS EBC, including: three of the DAVIS346 (SN 0249, SN 0253, and SN 0498), and one DVXplorer (SN DXA00063). Taking the PPS signal as ground truth for the passage of exactly one second, the index of generated triggers can be compared to each associated timestamp to determine clock drift. Each 24-hour dataset was divided into 24 single-hour data sets from which the clock drift was measured. Each camera showed a near constant drift (albeit at different rates for each model/serial number) and the hour-long cumulative drift could be accurately approximated using linear regression. A clock drift rate for each EBC was determined by averaging the rates calculated from each hour-long subset of the full 24-hour data collection. The mean drift per EBC timestamp digital resolution (1 μsec) can then be used as a correction factor to subtract out calibrated drift from each recorded change event timestamp. Thus, any future event data can be correlated to real (absolute) time using the known correction factor determined for each EBC assuming the computer clock has been synchronized to absolute time to within some fraction of a second.

During three out of the four 24-hour recordings, either the GPS receiver briefly lost connection and failed to send a pulse or the EBC malfunctioned and did not detect one or more input pulses. Although these malfunctions were brief and the system recovered to continue recording as before, the extended delay between reported PPS detections created gaps in the data that negatively affected the linear fit. As such, hour-long data subsets in which these gaps occurred were not used in the final calculation of the mean correction factor. SN 0253 suffered the most affected data subsets (3 out of the total 24), while SN 0498 was the only camera that did not experience any data gaps during its 24-hour recording.

4. RESULTS

This section presents refractory period estimation results for the gen4 EVKv2 and gen4 EVKv3, well as an initial empirical demonstration of a novel approach to pixel bandwidth measurement using gen4 data captured while viewing a static scene. We also present our initial clock drift measurements for the DAVIS346 and DVXplorer, including results for simple mean drift correction.

4.1 Refractory period evaluation using a controlled dynamic scene

gen4 EVKv3

Table 4 summarizes the six gen4 EVKv3 data sets recorded using simple variations of the basic setup shown in Figure 3. The first data set recorded all pixels using a red LED source as input to the integrating sphere, with a chopper wheel providing 20 Hz modulation, and using the smaller of two distances separating light source and camera (≈80 cm). Results for this data set presented earlier in Section 3 show saturation of mean minimum ISI (within analysis ROI) near 60 μsec coinciding with readout saturation at the default 20 Meps enforced by the on-chip ERC. All subsequent data sets used a bright white LED operating at maximum current, a 4 Hz chopper wheel induced modulation, and the on-chip ERC remained at default (20 Meps). These additional data sets explored simple excursions on range (≈2× further or 1.6 m in some cases) and sensor ROI as controlled by the MetaVision software.

Expanding on Figure 6, mean minimum ISI is plotted in Figure 9 versus refractory period bias setting for all six data sets listed in Table 4. Total mean event rate is plotted separately for these six data sets in Figure 10. The mean min ISI curve resulting from data set number two yields the overall minimum curve (note that data was not collected at *refr_bias* = 20 for 3 of 6 data sets) and shows a smooth monotonic decrease as *refr_bias* increases to its maximum value of 100. The mean min ISI values from data set 2 range from 1.6 msec to 11.3 μsec at *refr_bias* values of 30 and 100, respectively. The

Table 4. Summary of gen4 EVKv3 data sets collected to explore refractory period estimation via mean minimum ISI.

Data Set	LED Source	Distance	Chopper Wheel Modulation (Hz)	MetaVision ROI (format)	MetaVision ROI (# pixels)	Analysis ROI (# pixels)
1	Red	close	20	Full sensor (720x1280 pix)	921600	4441
2	Bright White	close	4	Reduced (150x150 pix)	22500	1257
3	Bright White	close	4	Full sensor	921600	1212
4	Bright White	close	4	Reduced (5x5 pix)	25	25
5	Bright white	far	4	Reduced (5x5 pix)	25	25
6	Bright White	far	4	Full sensor	921600	445

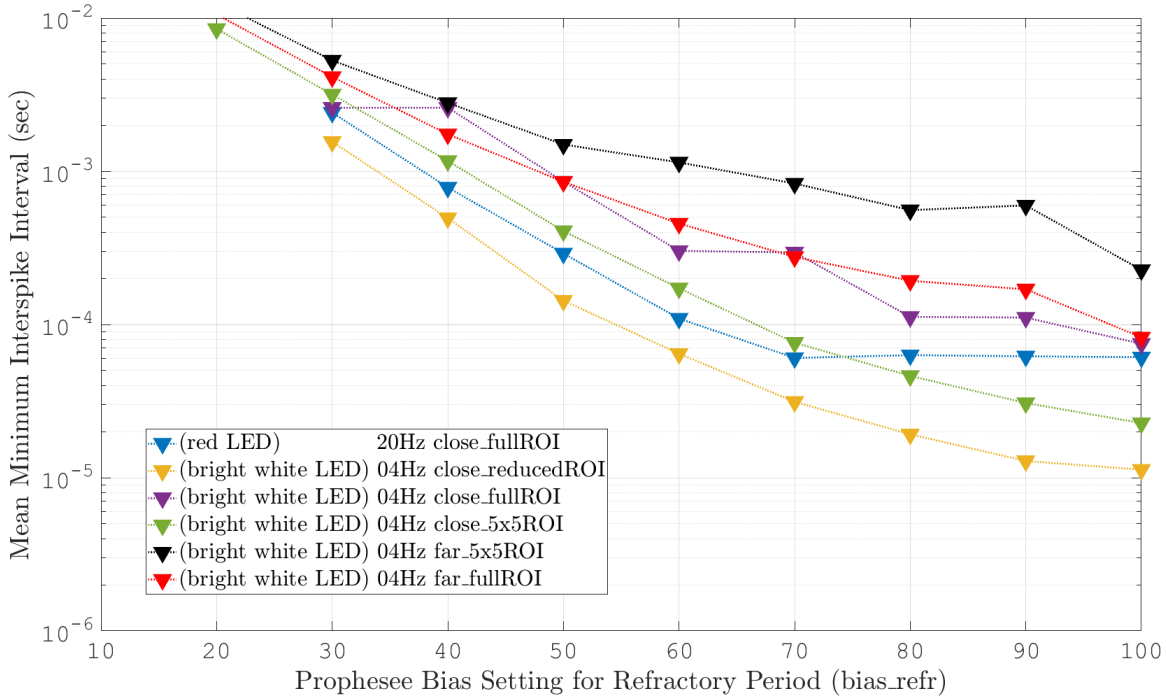

Figure 9. Prophesee gen4 EVKv3 mean minimum (per-pixel) interspike interval within an analysis ROI isolating pixels imaging the integrating sphere output port through chopper wheel blade – as a function of refractory period bias setting, *bias_refr*, which was adjusted using the Prophesee MetaVision software.

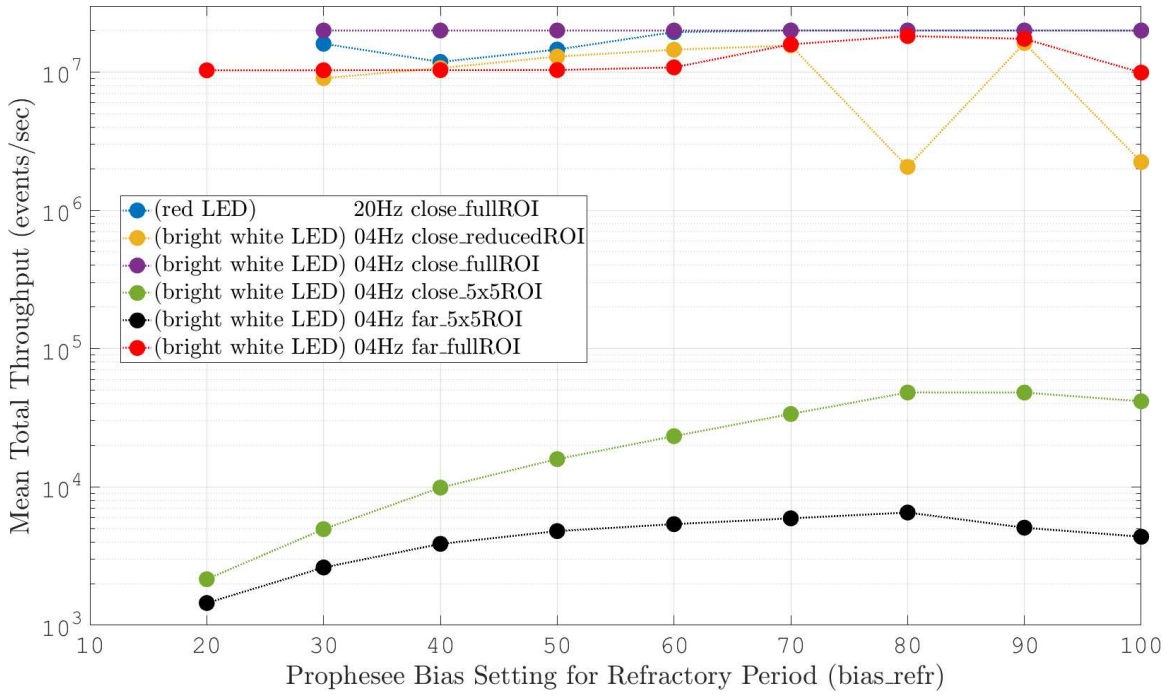

Figure 10. Prophesee gen4 EVKv3 mean event throughput (across file duration) as a function of refractory period bias setting, *bias_refr*, which was adjusted using the Prophesee MetaVision software.

total mean event throughput for this data set shows some oscillating behavior for *refr_bias* values greater than 70, but the total mean throughput remains at least slightly below 20 Meps for all values of *refr_bias* exercised. Based on visual inspection of Figure 10, the two data sets captured using the full sensor format and at the shorter range both exhibit readout saturation (for some or all *refr_bias* values exercised). Note also from Figure 10 the two sets captured using the smallest exercised ROI of only 25 pixels yield a much-reduced mean throughput of less than 100 Keps for all settings exercised.

gen4 EVKv2

Several gen4 EVKv2 (S/N 0000a4f4) data sets were collected using a separate setup from that used for testing the EVKv3. For the EVKv2, we used a testbed based on the SpectralLED integrating sphere from Gamma Scientific as described in Sect. 3 and previously reported [13]. Several EVKv2 data sets were collected using a chopper wheel to provide a 4 Hz light source modulation. This setup allows a programmable radiometric light source not provided by our earlier setup used for the EVKv3, enabling automated data acquisition and estimation of mean minimum ISI curves for controlled light levels. Mean minimum ISI results are presented in Figure 11 for the case of using a 50x50 pixel MetaVision ROI to reduce risk of readout saturation, and using the same bias settings as for the EVKv3 (listed in Table 2) to maximize both (1) bandwidth upstream from comparator, and (2) change detection sensitivity (minimum contrast thresholds). However, unlike for the EVKv3 data sets, all EVKv2 data sets reported herein were for the case where the ERC was set to maximum and then disabled, in which case the total sustained throughput is nominally limited to about 1 Geps [2].

For the five light levels employed, visual inspection of the empirical mean min ISI curves of Figure 11 indicates both (1) a downward trend of mean min ISI with increasing *bias_refr* value, and (2) a downward shift of the entire curve with increasing light level up to about 5%, then little change going from 5% to 10% (of max SpectralLED output). On-chip illuminance at 5% max light level is approximately 41.5 lux. The mean min ISI values at 5% max light level range from 6.1 msec to 6.8 µsec at *bias_refr* values of 20 and 100, respectively. Note that initial post-processing yielded erratic mean min ISI curves inconsistent with visual inspection of the underlying histograms. As an example, log-histograms of the minimum per-pixel ISIs within the analysis ROI are displayed in Figure 12 Figure 5for data collected at 5% max light level. There are a significant number of min ISI values of 1 microsecond (the digital timestamp resolution) which in some cases was noticeably biasing the mean values of the visually inspected histograms. Therefore, all min ISI values of 1 microsecond were ignored, and all data re-processed prior to reporting mean min ISI values in this paper.

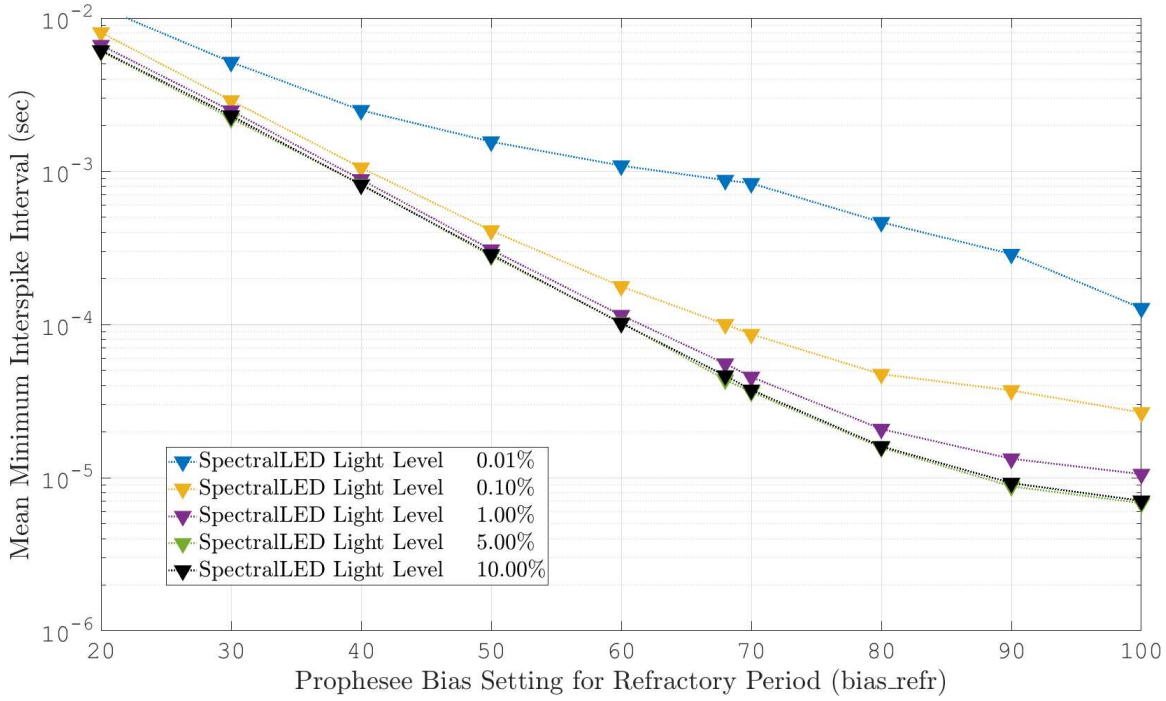

Figure 11. Prophesee gen4 EVKv2 mean minimum interspike interval within a 50x50 analysis ROI isolating pixels imaging the integrating sphere output port through 4 Hz chopper wheel blade – as a function of refractory period bias setting, *bias_refr*.

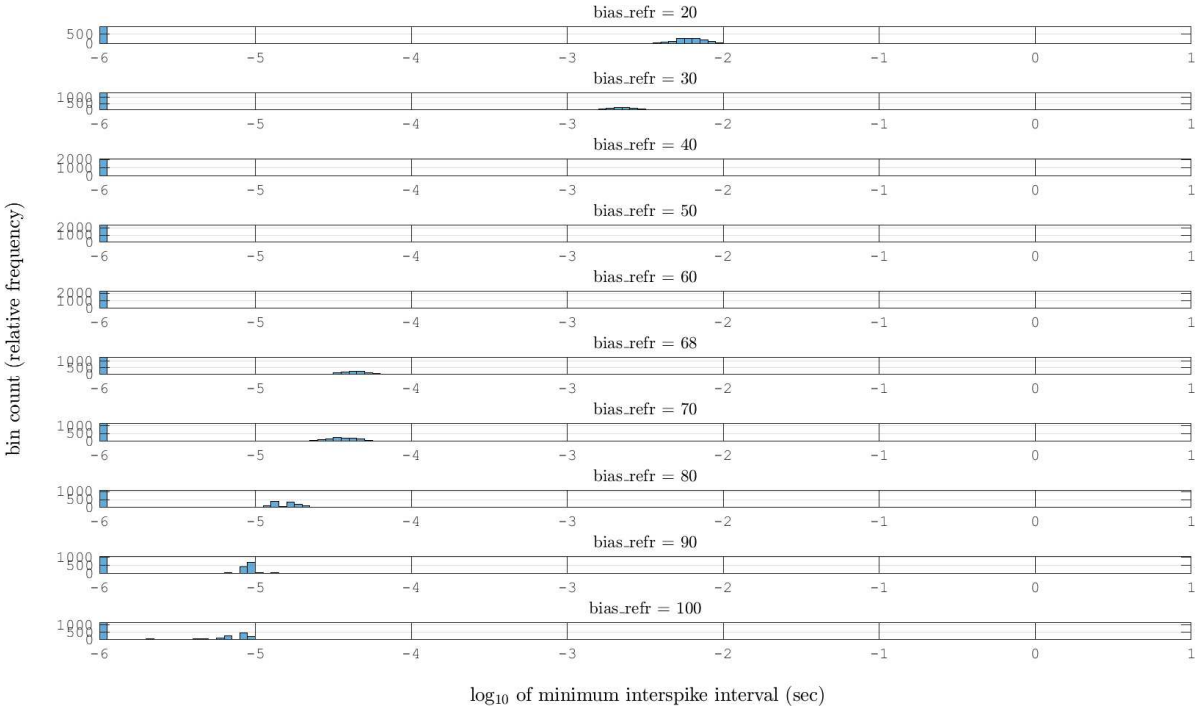

Figure 12. Base-10 log-histograms of the minimum per-pixel ISIs within a 50x50 pixel MetaVision ROI for the EVKv2 viewing SpectralLED at 5% of max light level (through a 4 Hz chopper wheel), for values of *bias_refr* ranging from slowest (20) at top to the fastest (100) at bottom.

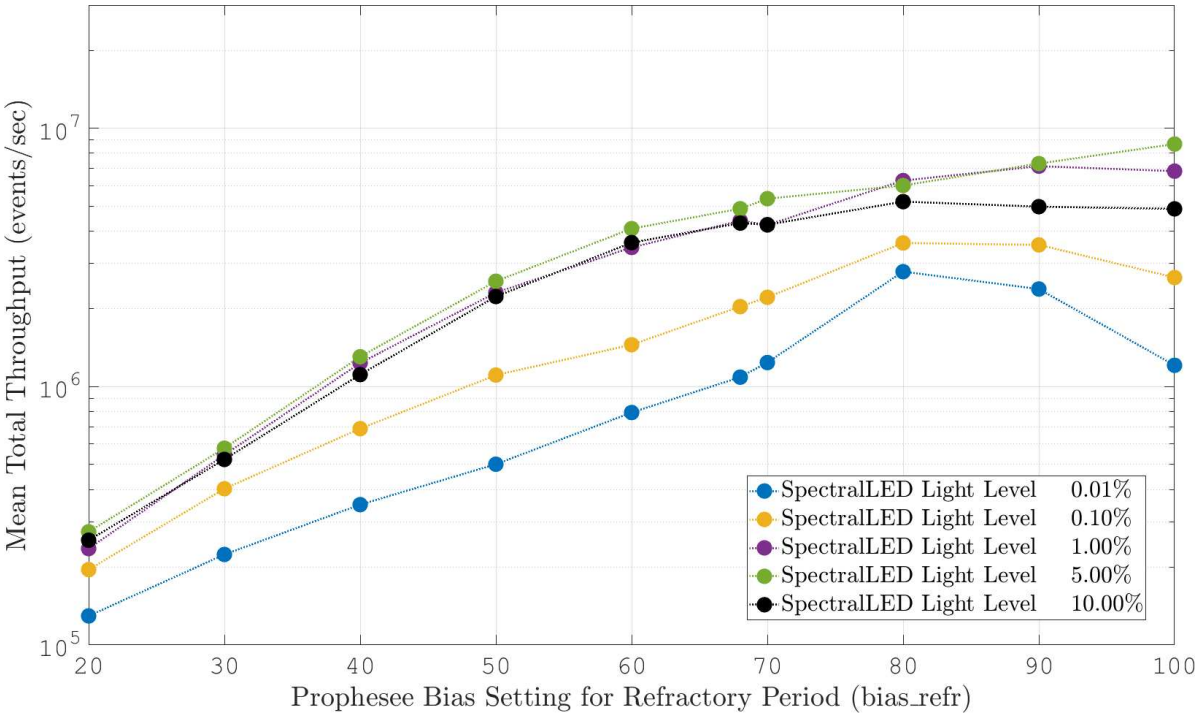

Figure 13. Prophesee gen4 EVKv2 mean event throughput as a function of refractory period bias setting, *bias_refr*.

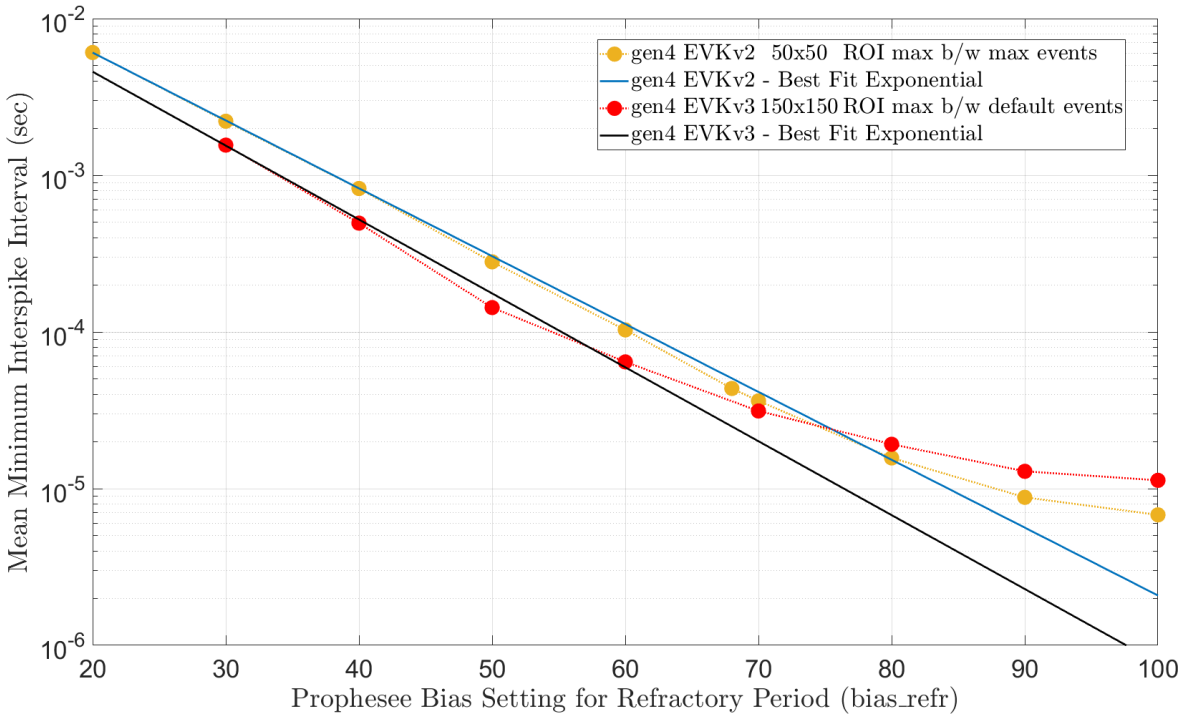

Figure 14. Visually best mean minimum (per-pixel) interspike interval measurements for the gen4 EVKv2 (gold circles) and gen4 EVKv3 (red circles) EBCs. The corresponding best fit exponential functions are also plotted as solid blue and black lines for the EVKv2 and EVKv3, respectively.

Corresponding curves for total mean event rate (across file duration) versus *bias_refr* are presented in Figure 13. Visual inspection of Figure 13 indicates an overall upward trend in event rate as *refr_bias* increases (toward smaller deadtimes), and the total mean event rate remains below 10 Meps for all exercised combinations of light level and *refr_bias* value – where the MetaVision ROI is 50x50 (2500 pixels) or 0.3% of the full FPA format in all cases. Note also that the mean total throughput curves initially shift upward with increasing light level, then show relatively little change for SpectralLED levels beyond 1% of max output.

Consolidated gen4 Results

The visually best mean min ISI curve for the gen4 EVKv2 is taken to be the 5% max light level curve from Figure 11 (nearly identical to the result for 10% max light level). The visually best mean min ISI curve for the gen4 EVKv3 is taken to be the result from data set 2 (Table 4) for the closest of two distances considered and using a reduced ROI (150x150 pix) but not the smallest ROI (5x5 pix) employed. Possibly the smallest ROI combined with the short duration files (≈1 sec recordings) did not provide sufficient data volume for accurate estimation of the mean min ISI. These two *visually best* curves are plotted together in Figure 14 along with corresponding best fit exponential functions of the form:

$$y(x) = Ae^{Bx} \tag{4}$$

The best fit exponential function for the EVKv2 is defined by A= 0.04458 and B = -0.09973 yielding an R^2 of 1.0000. The best fit exponential function for the EVKv3 is defined by A = 0.04018 and B = -0.1086 yielding an R^2 of 0.9988. For the EVKv2, the best fit exponential closely matches the data for *refr_bias* values of 20 through 80, with measurements diverging (and increasingly so) from the best fit curve for *refr_bias* values of 90 and 100. For the EVKv3, the best fit exponential closely matches the data for *refr_bias* values of 30 through 60 (data was not collected at *refr_bias* = 20), with measurements diverging (and increasingly so) from the best fit curve for *refr_bias* values of 70 through 100.

4.2 Measuring front-end pixel bandwidth using a static scene

Monte Carlo simulations of a single DVS pixel using a custom tool based on the open-source DVS simulator V2E [20] yielded the set of data points seen in Figure 15. The y-axis is the fraction of opposite polarity ISIs and the x-axis is the ratio of refractory period to the time constant of the simplified front-end pixel filter model. Each point represents the mean value from 500 runs, each consisting of 30 seconds of simulator output in response to a pure Gaussian white noise input

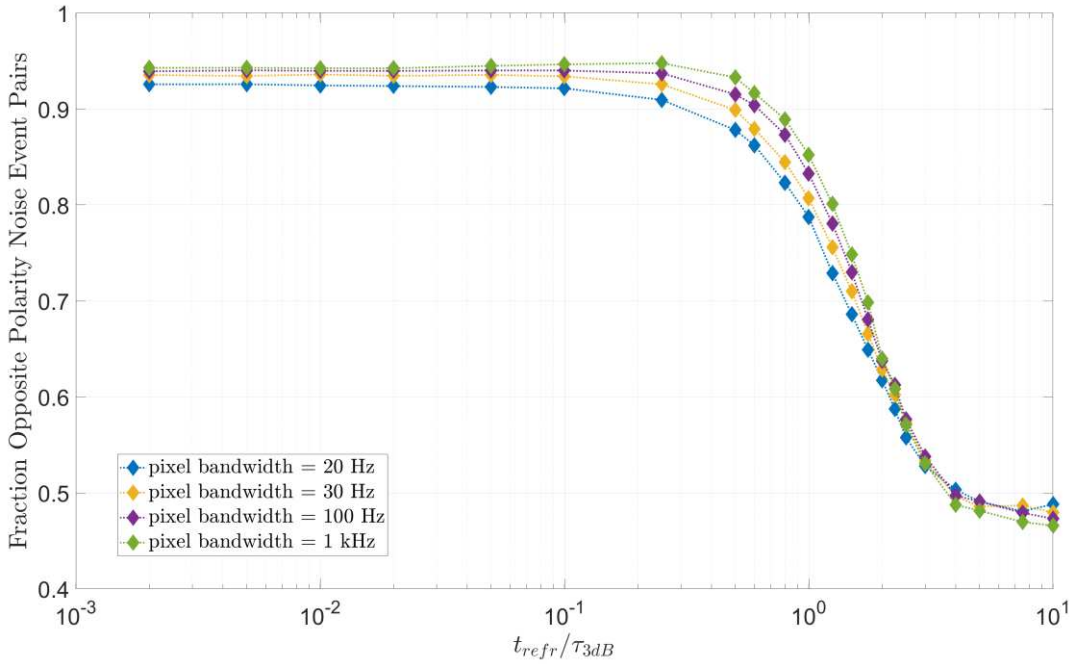

Figure 15. Monte Carlo simulations of a single DVS pixel showing noise-event de-coupling in terms of fraction of total event pairs being opposite polarity as a function of the ratio of refractory period to time constant of the simplified pixel filter model.

signal. A temporal resolution of 10 μsec was used for the generated noise signal. Simulation results are presented for four different cut-off frequencies (20, 30, 100, and 1000 Hz) where the noise power was adjusted so that overall noise event-rate was approximately the same for each f_{3dB} value modeled. The result of Figure 15 indicates that noise-event pairs become decoupled (i.e., the fraction of opposite polarity pairs drops to 0.5), when $t_{refr}/\tau_{3dB} \approx 4$. In total, 8 simulated curves were generated for varied f_{3dB} values ranging from 10 Hz to 1 kHz. Across all 8 settings, the curves were observed to converge at the point on the x-axis corresponding to $t_{refr}/\tau_{3dB} = 4$ where the mean and standard deviation of the fraction of opposite-polarity event pairs at this point was 0.4986 ± 0.0052.

An initial empirical demonstration of noise-event decoupling is presented in Figure 16 for data captured by the Prophesee gen4 EVKv2 viewing a static scene (inside light-tight enclosure) – in this case viewing the SpectralLED integrating sphere operating at 0.05% max light level (chopper wheel removed). For the given 25 mm f/4.0 lens, this corresponds to about 0.36 lux on-chip. The MetaVision ROI feature was employed to limit data acquisition to 160K pixels (400x400 pixel ROI), and the (object) distance between the camera and integrating sphere output port was about 26 cm. A one-minute data acquisition was recorded at each data point (*refr_bias*, *bias_fo*), then analyzed to find the fraction of ISIs being opposite polarity (ON→OFF or OFF→ON). Measured curves for fraction opposite polarity (noise event pairs) as a function of refractory period bias setting are presented in Figure 16 for seven different values of the bias setting *bias_fo* (low-pass filter, see Table 2) spanning the entire range of parameter values. In this case, the observed de-coupling occurs at a refractory period bias setting near 30 for all seven low-pass filter settings exercised. From our mean min ISI results (Figure 14), this corresponds to a physical refractory period of about 2.2 msec. Combined with our DVS circuit simulation results, this implies a front-end pixel bandwidth of about 288 Hz. In our result, all seven curves converge to nearly the same 50% event pair fraction opposite polarity point, indicating that the bandwidth is nearly identical for the seven settings evaluated. Given that the measurements were taken under moderate lighting conditions (0.36 lux on-chip), this result is expected and indicates that the photocurrent level is limiting the speed of the system response, and not the low-pass filter.

The measurements behind Figure 16 were repeated for a higher light level of 0.5% max SpectralLED output. The corresponding curves for fraction opposite polarity versus *bias_refr* are presented in Figure 17 for five values of pixel bandwidth *bias_fo*. In this case, the on-chip illuminance is roughly 4.16 lux and the bandwidth estimate is about 2.16 kHz (the group of curves crosses 50% near *bias_refr*=50.33). The fact that estimated bandwidth has increased with light level is consistent with the well-documented DVS pixel behavior.

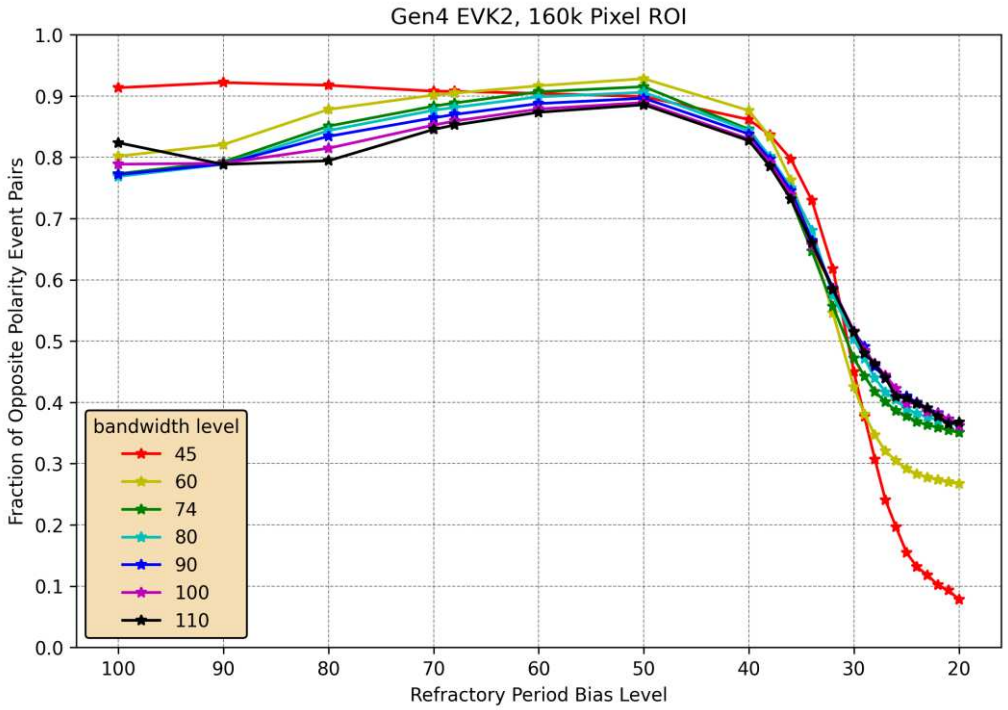

Figure 16. Empirical demonstration of noise event de-coupling using the Prophesee gen4 EVKv2 attached to a 25 mm f/4.0 lens viewing a static scene (SpectralLED operating at 0.05% max output). On-chip illuminance is approximately 0.36 lux.

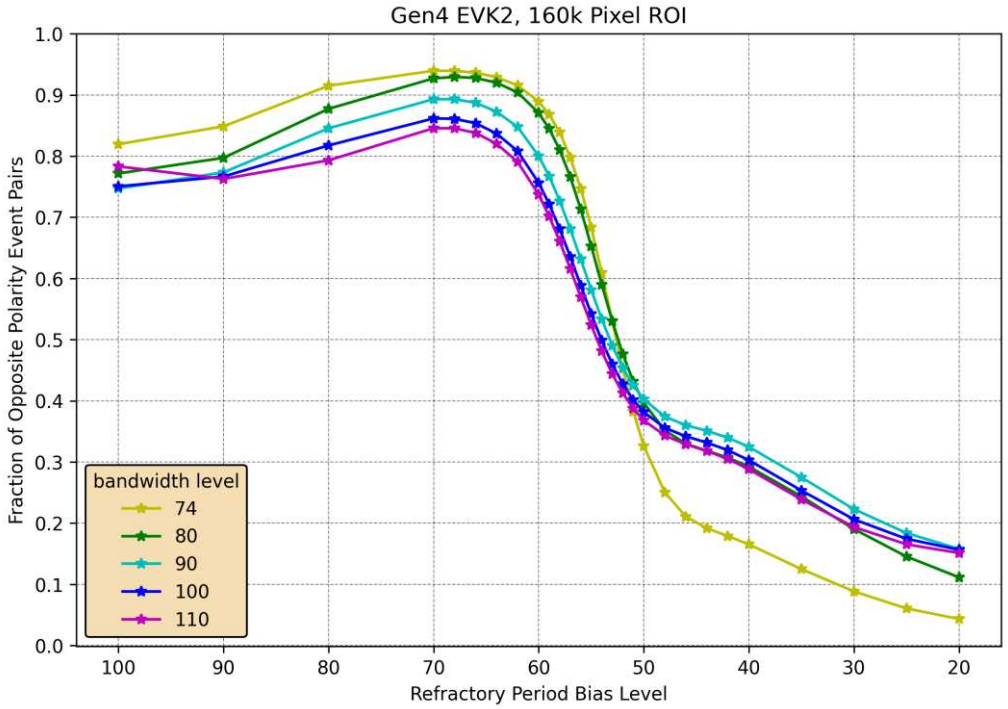

Figure 17. Empirical demonstration of noise event de-coupling using the Prophesee gen4 EVKv2 attached to a 25 mm f/4.0 lens viewing a static scene (SpectralLED operating at 0.5% max output). On-chip illuminance is approximately 4.16 lux.

Table 5. Measured clock drift rates (per unit clock time) and standard deviations for several EBCs from iniVation.

Camera Model and Serial #	Mean (1st set)	Std Dev (1st set)	Mean (2nd set)	Std Dev (2nd set)
DAVIS346 SN 0249	0.0099165	4.03E-07	0.0099114	5.64E-07
DAVIS346 SN 0253	0.0099177	3.88E-07	0.0099155	4.66E-07
DAVIS346 SN 0498	1.03E-05	5.57E-07	9.98E-06	5.88E-07
DVXplorer SN DXA00063	1.79E-05	3.08E-07	2.03E-05	7.54E-07

4.3 Initial measurement and correction of iniVation EBC clock drift

Clock drift for each evaluated COTS camera was determined by taking the difference between consecutive timestamps and one second (taking the spacing between adjacent PPS stimuli as ground truth for the passage of one second). The resulting array of drift values was cumulatively summed so that deviation from real time could be tracked as a function of raw timestamp value. Average drift rates (and standard deviations) are reported in Table 5 along with results for a second group of 24-hour data sets recorded several weeks later, showing a slight deviance in draft rates over time. The drift rates are displayed in units of drift per unit of EBC timestamp (digital resolution), for example, 0.0099165 µs of drift are accumulated with every passing one µs tick of the SN 0249 clock. Future data corrections are as simple as using the measured drift rate to subtract out accumulated drift from each timestamp entry in a given [**x**,**y**,**p**,**t**] event-list data set. As points of reference, the mean drift rates from the first data sets equate to accumulated timing errors at 24 hours of 857 sec for both SNs 0249 and 0253, 0.9 sec for SN 0498, and 1.5 sec for SN DXA00063.

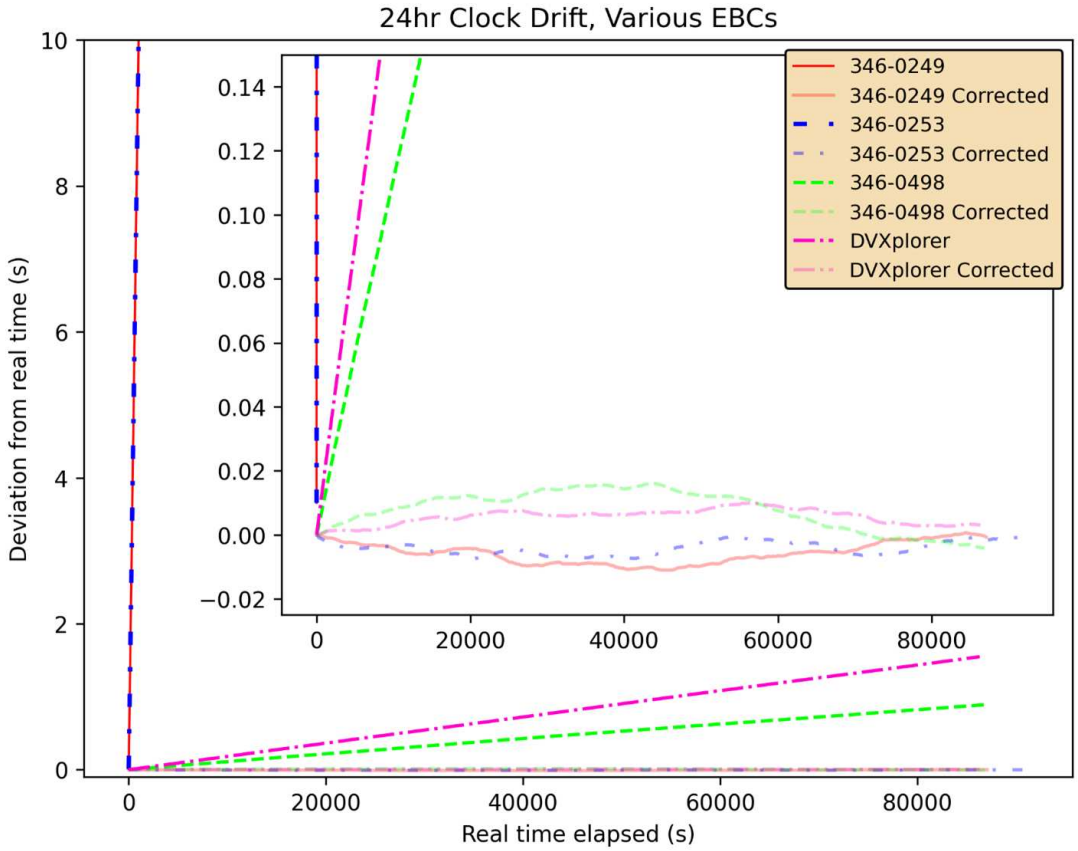

Figure 18. Accumulated drift as a function of real time elapsed is shown with pre-correction data in bold color and post-correction data in light color (results are for the first group of 24-hour data sets). SN 0249 and SN 0253 reach a maximum deviation of over 800 seconds by the end of the 24-hour recording (not shown). Inset: axes are zoomed to show the maximum deviation of (post-correction) residual jitter.

Table 6. Residual (post-correction) clock drift statistics (in milliseconds) for the first group of 24-hours data sets used to determine the mean drift rates shown in Table 5.

Camera Model and Serial #	Mean (msec)	Max Absolute Deviation (msec)	Std Dev (msec)
DAVIS346 SN 0249	-5.76	11.03	3.33
DAVIS346 SN 0253	-4.15	7.38	2.07
DAVIS346 SN 0498	+7.88	16.24	6.11
DVXplorer SN DXA00063	+5.68	10.01	2.37

Corrections to the first group of 24-hour trigger data were then (self) applied using the rates reported in Table 5. These are the same 24-hour data sets that were split into hour-long slices and averaged to determine a drift rate for each camera. The accumulated drift for raw and corrected (calibrated) timestamp data over a 24-hour period for each EBC is presented in Figure 18, along with a zoomed inset to magnify the residual jitter of post-correction timestamp data. Additionally, Table 6 summarizes post-correction clock drift statistics, with mean deviation from real time ranging from -5.8 msec to +7.9 msec, and maximum absolute deviation ranging from 7.4 msec to 16.2 msec, depending on the model and serial number. This residual jitter is likely a direct carryover from the jitter of the internal clock itself and thus cannot be subtracted out. We have not explored dependence on temperature.

Using the same drift rates determined from the first group of 24-hour datasets and reported in Table 5, corrections were applied to the second group of 24-hour datasets recorded several weeks later (Method 1). Figure 19 compares the results of using the first group drift rates as correction factors for the unassociated second group datasets, versus using the new drift rates (also provided in Table 5) determined from the second group datasets (Method 2). Though there exist only slight differences between the two sets of drift rates (i.e., clock calibration factors), substantial residual drift remains when applying the first group drift rates as a correction to the unassociated second group datasets (Method 1). Residual drift was determined by performing a linear regression on each hour of the dataset and averaging the rates. Table 7 reports the values of this residual drift for Method 1 as well as the clock jitter remaining post Method 2.

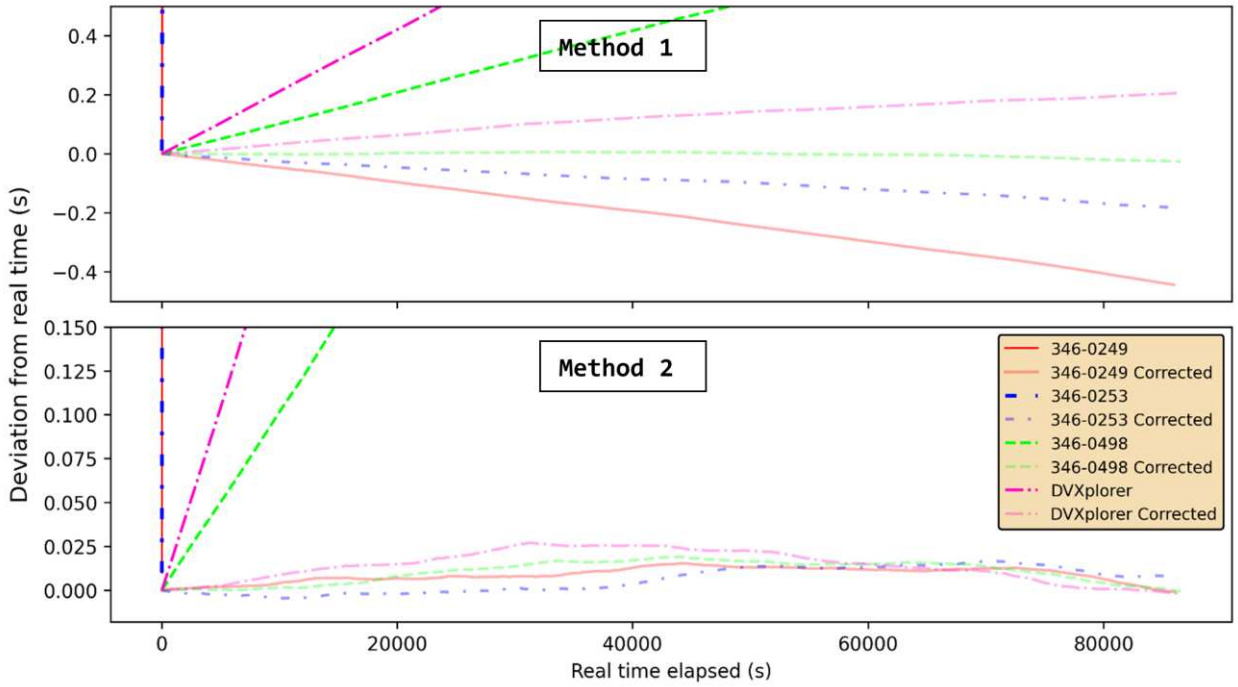

Figure 19. Method 1: mean drift rates from Dataset 1 were applied as corrections to Dataset 2 for each camera – remaining drift is apparent. Method 2: mean drift rates from Dataset 2 were used as corrections on the same datasets – only clock jitter remains.

Table 7: Residual Drift and Clock Jitter Post Methods 1 and 2.

	Method 1		Method 2		
Camera Model and Serial #	**Residual Drift (per unit clock time)**	**Residual Drift (msec/24hrs)**	**Mean Residual Jitter (msec)**	**Max Abs Dev (msec)**	**Std Dev (msec)**
DAVIS346 SN 0249	-5.11E-06	-440	8.81	15.29	4.15
DAVIS346 SN 0253	-2.15E-06	-190	5.87	16.67	7.06
DAVIS346 SN 0498	-2.87E-07	-25	11.24	19.94	6.44
DVXplorer SN DXA00063	+2.42E-06	+21	13.96	26.93	8.7

5. SUMMARY AND DISCUSSION

Unlike the well-developed and standardized photon transfer curve techniques used to characterize CCD/CMOS framing sensors and cameras, complementary methodologies appropriate for EBCs are still in research and development. In this paper we explored the utility of sweeping refractory period while viewing both static and dynamic scenes, then analyzing the event-list data focused on interspike interval (ISI) statistics to estimate pixel deadtime (refractory period) and potentially garner an indirect measure of front-end pixel bandwidth.

For the case of sweeping the refractory period bias setting while viewing a controlled dynamic scene, we demonstrated the feasibility of using mean minimum ISI as a model-free estimate of physical refractory period. This approach relies on:

- Introducing a relatively slow stimulus to a small fraction of the full event-sensor format – we primarily used a chopper wheel to impose a 4 Hz modulation on a static integrating sphere light source
- Ability to maximize front-end pixel bandwidth by controlling biases and light level
- Ability to record events from only a region-of-interest to avoid stressing readout/arbiter throughput limits
- Awareness and management of outliers – we removed all mean min ISI values of exactly one microsecond (one EBC clock tick) as these were obviously biasing the mean value in multiple data sets

For the state-of-the art gen4 EBC from Prophesee and Sony, the visually best measured mean min ISI curves are well modeled by an exponential function. For our tests of the gen4 EVKv2, the refractory period estimates range from 6.1 msec to 6.8 µsec going from the slowest (20) to fastest (100) settings of the relevant bias parameter *bias_refr*. Future work includes a closer examination of transition type in cases where min ISI equals one or a few microseconds.

For the case of sweeping refractory period while viewing a static scene, we presented both simulation and empirical results validating a novel approach to measuring EBC pixel bandwidth based on analyzing noise-event statistics. This approach relies on Monte Carlo simulations using a simplified circuit model to determine the ratio of refractory period to pixel front-end time constant such that noise-events become de-coupled and the fraction opposite-polarity noise-event pairs drops to 50%. Monte Carlo simulations of the DVS pixel show this de-coupling ratio to be a factor of four. Measurements using the Prophesee gen4 EVKv2 empirically demonstrate that this effect can be observed with real-world sensor output. For the EVKv2, noise event pair de-coupling occurs at a refractory period bias setting of about 30 for a SpectralLED light level of 0.05% max (roughly 0.36 lux on-chip). From our mean min ISI results, this corresponds to a physical refractory period of 2.2 msec. Combined with our circuit modeling result, this implies a front-end pixel bandwidth (for the given set of conditions) of 288 Hz. The EVKv2 measurements were then repeated at a higher SpectralLED light level of 0.5% max (roughly 4.16 lux on-chip) yielding a bandwidth estimate of 2.16 kHz. This result increases our confidence in the validity of this method, as it matches closely with the near linear increase in photoreceptor bandwidth as a function of illumination as predicted by small signal circuit analysis of the photoreceptor [23].

This approach allows measuring bandwidth without use of a modulated light source, potentially enabling a simpler characterization setup. However, appropriate light level and bias settings are required, and the approach depends on ability to program relatively slow refractory periods. For these measurements to inform true capabilities of the EBS, care must be taken to adjust the tunable front-end biases (typically referenced as photoreceptor and source follower) to ensure the signal bandwidth and noise bandwidth are the same. In practical use cases, this is optimal for noise reduction; however, the physics governing photoreceptor noise has only recently been reported. Graca, *et. al*., show that the minimum noise limit for dim lighting conditions is 2x the photon shot noise, and to achieve this performance, the photoreceptor bias must be increased, and the source follower decreased such that the dominant pole of the system transfer function is determined by the source follower [24]. Therefore, this approach likely complements the typically reported method and future work will include comparing bandwidth estimates from noise-event de-coupling with those obtained by viewing a light source

modulated with a periodic signal (such as a sine wave) at increasing frequencies and monitoring the average number of events generated per cycle.

Finally, our results indicate that event data timestamp correction is possible and effective for the COTS VIS EBCs from iniVation using a simple test setup and constant drift rate model to measure and correct for clock drift (perform drift subtraction). Although residual internal clock jitter remains a factor, the accuracy of post-correction event timestamps in relation to their real-time occurrence will now allow events to be linked to their outside stimuli. Determining the drift rate from the same data on which subtraction is performed results in mean jitter ranging from about 4-14 ms (±2-9 ms) over a 24-hour period depending on the camera selected. Extrapolating the calculated drift rates for use on new and unassociated datasets yields less optimal results (remaining drift of up to ~5E-06 per unit clock time, or roughly half a second of drift per 24 hours), though it may still be an effective method for a course first-correction or for use on datasets covering shorter periods of time. The most effective system going forward likely involves consolidating the test setup constituents into a concise package that can accompany any astrometric data collect allowing EBC clock calibration to be determined on a per dataset basis. Inspection of the clock drift and jitter of Prophesee EBCs would serve as a useful future analysis, informing the end user of timing performance tradeoffs between event-based sensing products from iniVation and Prophesee.

ACKNOWLEDGEMENTS

We thank the OSD/FCT Program for partial support of this research.

REFERENCES

[1] Mahowald, M., "VLSI analogs of neuronal visual processing: a synthesis of form and function," PhD Thesis, California Institute of Technology (1992).

[2] Gallego, G., Delbrück, T., Orchard, G., Bartolozzi, C., Taba, B., Censi, A., Leutenegger, S., Davison. A. J., Conradt, J., Daniilidis, K., and Scaramuzza, D., "Event-based Vision: A Survey," in *IEEE Trans. Pattern Anal. Mach. Intell.* **44**(1), 154-180 (1 Jan 2022). https://doi.org/10.1109/TPAMI.2020.3008413.

[3] Finateu, T., Niwa, A., Matolin, D., Tsuchimoto, K., Mascheroni, A., Reynaud, E., Mostafalu, P., Brady, F., Chotard, L., LeGoff, F., Takahashi, H., Wakabayashi, H., Oike Y., and Posch, C., "A 1280×720 Back-Illuminated Stacked Temporal Contrast Event-Based Vision Sensor with 4.86µm Pixels, 1.066GEPS Readout, Programmable Event-Rate Controller and Compressive Data-Formatting Pipeline," *2020 IEEE International Solid-State Circuits Conference (ISSCC)*, San Francisco, CA, 112-114 (2020). https://doi.org/10.1109/ISSCC19947.2020.9063149.

[4] Cohen, G., Afshar, S., van Schaik, A., Wabnitz, A., Bessell, T., Rutten, M., and Morreale, B., "Event-based sensing for space situational awareness," *Advanced Maui Optical and Space Surveillance Technologies Conference*, Maui, Hawaii, USA, September 2017.

[5] McMahon-Crabtree, P. N., and Monet, D. G., "Commercial-off-the-shelf event-based cameras for space surveillance applications," *Appl. Opt.* **60**(25), G144-G153 (2021). https://doi.org/10.1364/AO.425623.

[6] European Machine Vision Association (EMVA), "EMVA Standard 1288: Standard Characterization of Imaging Sensors and Cameras," Release 4.0 General, 16 June 2021. www.emva.org.

[7] Janesick, J. R., Klaasen, K. P., and Elliott, T., "Charge-Coupled-Device Charge-Collection Efficiency and The Photon-Transfer Technique," *Opt. Eng.* **26**(10) 261072 (1 October 1987). https://doi.org/10.1117/12.950297.

[8] Janesick, J. R., [Photon Transfer DN→λ], SPIE Press, Bellingham, WA (2007). https://doi.org/10.1117/3.725073.

[9] Joubert, D., Hébert, M., Konik, H., and Lavergne, C., "Characterization setup for event-based imagers applied to modulated light signal detection," *Appl. Opt.* **58**(6), 1305-1317 (2019). https://doi.org/10.1364/AO.58.001305.

[10] McReynolds, B., Graca, R., and Delbruck, T., "Experimental methods to predict dynamic vision sensor event camera performance," *Opt. Eng.* **61**(7), 074103-1 – 074103-19 (July 2022). https://doi.org/10.1117/1.OE.61.7.074103.

[11] Graca, R., and Delbruck, T., "Unraveling the paradox of intensity-dependent DVS pixel noise," in arXiv [eess.SY] (2021). https://doi.org/10.48550/arXiv.2109.08640.

[12] Roffe, S., Akolkar, H., George, A. D., Linares-Barranco, B., and Benosman, R. B., "Neutron-Induced, Single-Event Effects on Neuromorphic Event-Based Vision Sensor: A First Step and Tools to Space Applications," *IEEE Access* **9**, 85748-85763 (2021). https://doi.org/10.1109/ACCESS.2021.3085136.
[13] McMahon-Crabtree, P. N., Pereira W., Crow, R., Preston, R., Kulesza, L., Crowell, R., Morath, C. P., Maestas, D., Theis, Z., and Sablan, P., "Automated characterization techniques and testbeds for event-based cameras," *Proc. SPIE* 12233, Infrared Remote Sensing and Instrumentation XXX, 122330B (30 September 2022); https://doi.org/10.1117/12.2634166.
[14] Guo, S., and Delbruck, T., "Low Cost and Latency Event Camera Background Activity Denoising," in *IEEE Trans. Pattern Anal. Mach. Intell.* **45**(1), 785-795 (1 Jan 2023). https://doi.org/10.1109/TPAMI.2022.3152999.
[15] McReynolds, B., Graca, R., and Delbruck, T., "Exploiting Alternating DVS Shot Noise Event Pair Statistics to Reduce Background Activity," in arXiv [eess.IV] (2023). https://doi.org/10.48550/arXiv.2304.03494.
[16] Lichtsteiner, P., Posch, C., and Delbruck, T., "A 128 × 128 120 dB 15 μs latency asynchronous temporal contrast vision sensor," *IEEE J. Solid-State Circuits* **43**(2), 566–576 (2008).
[17] Posch, C., Serrano-Gotarredona, T., Linares-Barranco, B., and Delbrück, T., "Retinomorphic Event-Based Vision Sensors: Bioinspired Cameras with Spiking Output," *Proc. of the IEEE* **102**(10), 1470-1484 (Oct 2014).
[18] Graca, R., McReynolds, B., and Delbruck, T., "Shining light on the DVS pixel: A tutorial and discussion about biasing and optimization," in arXiv [eess.IV] (2023). https://doi.org/10.48550/arXiv.2304.03494.
[19] Nozaki, Y., and Delbrück, T., "Temperature and Parasitic Photocurrent Effects in Dynamic Vision Sensors," *IEEE Trans. Electron Devices* **64**(8), 3239-3245 (Aug 2017).
[20] Hu, Y., Liu, S-C.and Delbrück, T., "v2e: From video frames to realistic DVS events," in *arXiv* preprint (2020). https://doi.org/10.48550/arXiv.2006.07722.
[21] Posch, C., and Matolin, D., "Sensitivity and uniformity of a 0.18μm CMOS temporal contrast pixel array," *Proc. 2011 IEEE International Symposium of Circuits and Systems (ISCAS)*, Rio de Janeiro, Brazil, May 2011, pp. 1572-1575, https://doi.org/10.1109/ISCAS.2011.5937877.
[22] Prophesee MetaVision SDK Documentation, https://docs.prophesee.ai/stable/hw/manuals/biases.html, accessed 22 May 2023.
[23] Delbrück, T., and Mead, C.A., "Analog VLSI Phototransduction by continuous-time, adaptive, logarithmic photoreceptor circuits," California Institute of Technology, Pasadena, CA (1995). (Unpublished) https://resolver.caltech.edu/CaltechAUTHORS:20150908-164952926.
[24] Graca, R., McReynolds, B., and Delbrück, T., "Optimal biasing and physical limits of DVS event noise," in 2023 International Image Sensor Workshop (IISW), May 2023. https://doi.org/10.48550/arXiv.2304.04019.